JOINT EUROPEAN TORUS JET

JET–P(93)100

W. Kerner, D. Borba, G.T.A. Huysmans, F. Porcelli,
S. Poedts, J.P. Goedbloed, R. Betti

Stability of Global Alfven Waves (TAE, EAE) in JET Tritium Discharges

Stability of Global Alfven Waves (TAE, EAE) in JET Tritium Discharges

W. Kerner, D. Borba, G.T.A. Huysmans, F. Porcelli,
S. Poedts[1], J.P. Goedbloed[1], R. Betti[2]

JET-Joint Undertaking, Culham Science Centre, OX14 3DB, Abingdon, UK

[1]FOM Institute for Plasma Physics, 'Rijnhuizen', Nieuwegein, The Netherlands.
[2]Lab. Laser Energetics, Un. Rochester, Rochester NY 14627, USA.

Preprint of a paper to be submitted for publication in
Plasma Physics and Controlled Fusion.
November 1993

ABSTRACT

The interaction of alpha particles in JET tritium discharges with global Alfvén waves via inverse Landau damping is analysed. It is found that α-particle driven eigenmodes were stable in the PTE1 and should also be stable in a future 50:50 D-T mix discharge aiming at $Q_{DT} \simeq 1$, provided the same ion density as in the discharges with best D-D performance is maintained.

1. INTRODUCTION

The gross macroscopic properties of a plasma concerning equilibrium and stability are well described by the theory of magnetohydrodynamics (MHD). However, energetic ions with energies in the MeV range need to be considered. Such energetic ions are generated in ignited plasmas as fusion products or by auxiliary heating and current drive.

The successful production of controlled thermonuclear energy using a deuterium tritium fuel mixture was achieved with the JET Tokamak experiment on the 9th November 1991. The total fusion releases were 1.7MW peak power and 2MJ of energy (JET Team 1992). The α-particle pressure was moderate, $\beta_\alpha = 1.5 \times 10^{-4}$, with a peaked value on axis of $\beta_\alpha\,(0) = 1.4 \times 10^{-3}$. In addition, RF heating has produced energetic tail ions in excess of 1MeV in JET.

Estimates on plasma transport yield confinement times which are compatible with ignition requirements. Consequently, additional fast losses as triggered by instabilities constitute the major limitation to α-particle confinement. Such anomalous diffusion can be caused by either collective instabilities or turbulence phenomena. Therefore, the MHD description valid for the background thermal plasma has to be enlarged to take into account the high-energy ions. This leads to a hybrid kinetic-MHD model. Obviously, the wave particle interaction where the parallel phase velocity is equal to the parallel particle velocity, i.e.

$$\frac{\omega}{k_\parallel} \sim v_\parallel \quad , \tag{1}$$

will play an important role. The velocity of α-particles

$$v_\alpha = \left(\frac{2E_\alpha}{m_\alpha}\right)^{1/2} \approx 1.3 \times 10^9 \text{cm/s} \rightarrow 7 \times 10^8 \text{cm/s} \qquad (2)$$

with E_α = 3.5MeV $\rightarrow$ 1MeV, where 1MeV constitutes an 'average' energy, can be equal to the Alfvén velocity, which for typical JET parameters, B = 2.8T and $n_D = n_T = 1.5 \times 10^{13}\text{cm}^{-3}$, is

$$v_A = \frac{B}{(\mu n_i m_i)^{1/2}} \approx 7 \times 10^8 \text{cm/s}. \qquad (3)$$

The study of MHD modes driven unstable by energetic particles due to additional heating and, in particular, by alpha particles is crucial for the prediction of α-confinement for future JET D-T discharges aiming at $Q_{DT} \simeq 1$. In this paper we analyse the toroidicity and elongation induced Alfvén eigenmodes (TAE, EAE), their damping and their destabilisation by energetic particles. The spectral code CASTOR (Complex Alfvén Spectrum for Toroidal Plasmas) (Kerner et al, 1991) provides the tool for the analysis of the ideal and dissipative MHD spectrum.

In section 2 the Alfvén spectrum for JET PTE discharges is discussed. In section 3 the hybrid kinetic - MHD model based on the approximation used by Betti and Freidberg is applied to the stability analysis of JET PTE1 discharges. Of special interest is the analysis of the best performance JET discharge which is considered for future D-T discharges aiming at break-even. The discussion and conclusions are eventually presented in section 4.

2. ALFVÉN SPECTRUM OF JET PTE DISCHARGES

Tokamak equilibria obey force balance in ideal MHD

$$\underline{J}_0 \times \underline{B}_0 = \nabla P_0, \qquad (4)$$

where $\underline{B}_0$ denotes the equilibrium magnetic field, $\underline{J}_0$ the current density and P_0 the pressure. Plasma waves and instabilities that govern the linear perturbations around the ideal static equilibrium are described by the normal-mode analysis. The resistive MHD equations in the low-pressure limit assume the form,

$$\rho_0 \frac{\partial \underline{v}_1}{\partial t} = (\nabla \times \underline{B}_1) \times \underline{B}_0 + (\nabla \times \underline{B}_0) \times \underline{B}_1, \qquad (5a)$$

$$\frac{\partial \underline{B}_1}{\partial t} = \nabla x \left(\underline{v}_1 \times \underline{B}_1\right) - \nabla \times \left(\eta \nabla \times \underline{B}_1\right). \qquad (5b)$$

The subscript 1 denotes an Eulerian perturbation. The resistivity, η, is assumed to be constant in the present paper. The system (5) is written in dimensionless form. The time is expressed in Alfvén transit times $t_A = R/v_A$ with v_A evaluated at the magnetic axis. The velocity is normalised to v_A and the resistivity to $\mu R\, v_A$.

Since the equilibrium quantities do not depend on the toroidal angle ϕ the separation ansatz in the flux co-ordinate system $\left(s = \sqrt{\psi}, \vartheta, \phi\right)$

$$f_1(s, \vartheta, \phi, t) = e^{\lambda t} e^{in\phi} \sum_{m=-\infty}^{+\infty} f_{1m}(s) e^{im\vartheta} \qquad (6)$$

is suitable for the perturbed quantities. Here λ is the eigenvalue. The imaginary part of λ corresponds to oscillatory behaviour, while a negative real part indicates damping and a positive real part yields an exponentially growing instability.

The MHD spectrum of JET discharges is analysed by linking the spectral code CASTOR and the equilibrium solver HELENA (Huysmans et al., 1991) with the JET equilibrium identification code IDENTD (Blum et al., 1990).

The shear Alfvén waves are basically incompressible. The instabilities emerge from this branch. Usually, the stable Alfvén branches exhibit continua corresponding to eigenmodes where every field line oscillates with its own frequency

$$\omega_A(s) = k_{\parallel}(s) v_A(s). \qquad (7)$$

The normal component is damped like t^{-1}. If a coherent oscillation is enforced within such a continuum, e.g. by antenna excitation, this 'friction' yields resonant absorption. This effect accounts for **continuum damping**.

The normal component of the velocity exhibits a logarithmic singularity. When the singular nature of the continuum modes is prescribed the remaining regular part is easily solved for locally on every flux surface. In this fashion a specific version of CASTOR, namely CSCAS by Poedts and Schwarz (1992), allows

efficient determination of the continuous spectrum. By means of a small dissipation this singularity gets regularised. Thus, the continuum damping can be computed by extending the solution properly into the complex plane in ideal MHD or by computing the limit of asymptotically small dissipation as done in this paper. Earlier, Poedts and Kerner (1991) have established the result that the quasimode is a normal-mode in resistive MHD, where the damping becomes independent of eta in the limit of vanishing resistivity.

Due to the continuum damping Alfvén waves are usually difficult to destabilise. A different situation can occur in a toroidal or elongated system with finite aspect ratio and/or significant elongation. In such a system the poloidal harmonics in Eq. (6) are coupled causing gaps in the continua (Kieras, Tataronis, 1982 and Cheng, Chance, 1984). For details we refer to Poedts et al. (1992) and references therein.

The Alfvén spectrum for the JET PTE1 (#26148) for a toroidal wave number n = 1 is displayed in Fig. 1. Here, the value of the safety factor is above unity, q(0) = 1.05, throughout the plasma, which is appropriate for the early stages of the discharge. Since the plasma pressure is not large the Alfvén branch is examined solely; this is done by using a small value for the ratio of the specific heats. Two gaps are important, the toroidicity induced at $\omega / \tilde{\omega}_A = 0.5$ (≈ 150kHz) and the elongation induced gap at $\omega / \tilde{\omega}_A = 1.0$; $\tilde{\omega}_A$ denotes the characteristic Alfvén frequency at the magnetic axis. The TAE/EAE are localised around the flux surface where $k_{\parallel m,n} = -k_{\parallel \tilde{m},n}$, which corresponds to a value of the safety factor at the gap position.

$$q_G = \frac{m + \tilde{m}}{2n} = \left(\frac{3}{2} \text{for } m = 1,\ \tilde{m} = 2 \text{ and } n = 1 \right). \tag{8}$$

The width of these gaps is proportional to the coupling. The oscillatory frequency at the gap position is given by

$$\omega_A = \frac{\ell}{2} \frac{v_A}{R q_G} \left(\tilde{m} = m + \ell \right). \tag{9}$$

Inside these gaps the two (or more) harmonics with equal amplitude can give rise to a standing wave, i.e. to a global discrete Alfvén wave. The corresponding

eigenfunction is regular but localised with the width being proportional to the coupling, i.e. to the aspect ratio $\varepsilon = r/R$ and elongation $\kappa = (e - 1)/e$. In the case of strongly varying equilibrium (q or ρ) profiles, several gaps occur radially and several discrete eigenfunctions can overlap radially.

For this X-point discharge with nearly parabolic density profile there are radially four gaps. Further, four discrete eigenmodes exist in each of the major gaps. Two are strongly damped but the remaining two TAE and EAE exhibit no continuum damping because the gaps corresponding to different poloidal mode numbers m thread through the plasma. For a high density pedestal near the plasma boundary, here simulated by the extreme case of constant density (broken lines in Fig. 1), the gaps are shifted relatively to each other. This yields finite damping. The magnitude of this continuum damping strongly depends on the magnitude of the singular component. In particular, the continuum damping for the discrete mode with frequency $\omega / \tilde{\omega}_A = 0.30$ is still weak $-\gamma / \omega_G = 10^{-3}$. Only for the discrete EAE with frequency $\omega / \tilde{\omega}_A = 1.0$, where the continuum couples to the leading harmonics, the damping is large $-\gamma / \omega_G = 6 \times 10^{-3}$. The continuum damping has been computed in the limit of asymptotically small resistivity as indicated in Fig. 2. It is evident that the damping becomes independent of η.

The Alfvén spectrum for this discharge #26148 with n = 3 is displayed in Fig. 3. Here q(0) is below unity at the time of maximum fusion yield. Again in this hot-ion type of discharge the density falls off strongly. Thus, two major gaps occur where the subsequent gaps thread through the plasma radially. The frequencies of the dominant global Alfvén eigenmodes are indicated in the figure. The corresponding eigenfunctions of a TAE and of an EAE mode with n = 3 and that of a TAE mode with n = 5 are presented in Fig. 3b and Fig. 4.

Since the mode with, Δ_n, of the discrete eigenmodes becomes narrower with increasing mode numbers ($\Delta_n \sim 1/n$), the interaction with the continua occurs dominantly in the side harmonics. This yields decreasing continuum damping. A residual damping due to the Landau interaction with thermal electrons and ions, electron collisions, etc. can be offset by the inverse Landau damping with alpha particles, resulting in unstable global Alfvén modes.

3. DESTABILISATION OF DISCRETE ALFVÉN EIGENMODES

The α-particles at high energy are not in thermodynamic equilibrium. Thus, they can drive MHD instabilities through the α-particle inhomogeneity as the free energy source. The energetic particles influence the MHD solution through the pressure tensor.

$$\underline{\underline{P}} = p_\perp I + (p_\parallel - p_\perp)\underline{b}\ \underline{b}. \tag{10}$$

The components of the hot pressure-tensor are defined by

$$\begin{Bmatrix} \delta p_\parallel \\ \delta p_\perp \end{Bmatrix} = \int d^3v \begin{Bmatrix} m v_\parallel^2 \\ \tfrac{1}{2} m v_\perp^2 \end{Bmatrix} F_1\left(\underline{R},\ v_\parallel, \tfrac{1}{2} v_\perp^2\right), \tag{11}$$

where F_1 denotes the perturbed distribution function.

The momentum balance for the perturbed quantities yields

$$\lambda \rho_o\ \underline{v}_1 = \left[\underline{j} \times \underline{B} - \nabla p\right]_{(1)} - \nabla \delta \underline{\underline{p}}_h(\lambda,\ \underline{r}). \tag{12}$$

In the limit of small pressure, P_{core} as well as P_{hot}, we can assume that the influence of F_1 on the current has been taken into account in the equilibrium current and safety factor profiles. Even then Eq. (12) poses a difficult nonlinear eigenvalue problem. Under the assumption of a small drive the hot particle pressure gradient yields small growth rates,

$$\gamma / \omega_G << 1, \tag{13}$$

whereas the hot particle inertia can be neglected

$$\delta\omega / \omega_G << 1 \text{ implying } \omega \approx \omega_G. \tag{13b}$$

Thus, the perturbative approach is justified with

$$\underline{v} = \underline{v}_{MHD} + \delta \underline{v} \approx \underline{v}_{MHD}. \tag{14}$$

Quadratic forms can be constructed with the contribution of $\delta\underline{\underline{P}}_h$ to the potential energy in addition to the usual δW_{MHD}

$$\delta W_h = \left\langle \xi_\perp^* \cdot \nabla \delta \underline{\underline{P}}_h \right\rangle = \int d^3r d^3v \left\{ \left(v_\parallel^2 + \tfrac{1}{2} v_\perp^2 \right) \underline{\kappa} \cdot \xi_\perp^* \right\} F_1, \qquad (15)$$

where $\underline{\kappa} = \underline{b} \cdot \nabla \underline{b}$ is the curvature of the magnetic field lines. The growth rate is then proportional to the imaginary part

$$\gamma \; \alpha \; \mathrm{Im} \left\langle \xi_\perp^* \cdot \nabla \delta \underline{\underline{P}}_h \right\rangle. \qquad (16)$$

It is emphasised that this kinetic-MHD model is no longer self-adjoint. Therefore, strict sufficient and necessary stability criteria, similar to the ideal MHD energy priniciple, do not exist (Porcelli et al., 1993). However, since the MHD part, δW_{MHD}, is dominant, and the hot particle contribution, δW_{hot}, small, approximate solutions are constructed. The instabilities derived in this fashion will also appear when the MHD and kinetic equation are both solved exactly.

The equilibrium distribution function, F_o, is a function of the invariants of the system. F_1 is found by integrating along the unperturbed particle trajectories. The leading order guiding-centre orbits yield the particles on flux surfaces moving parallel to $\underline{B}$. In the usual tokamak ordering it holds that

$$\nabla \cdot \xi_\perp + 2 \, \underline{\xi}_\perp \cdot \underline{\kappa} \sim O(\varepsilon^2). \qquad (17)$$

It is furthermore sufficient to take the curvature $\underline{\kappa}$ as

$$\underline{\kappa} = -\underline{e}_R / R_o. \qquad (18)$$

As derived in more detail by Betti and Freidberg (1992) δW_{hot} is proportional to

$$\delta W_h \propto \int v_\perp \, dv_\perp \left(v_\parallel^2 + v_\perp^2 / 2 \right)^2 \left(\omega_G \frac{\partial F_o}{\partial E} - n / q_G \frac{\partial Fo}{\partial \psi} \right), \qquad (19)$$

with $v_\parallel$ given by the resonances. It is emphasised that with Eq. (6) and Eq. (18)

$$\underline{\xi}_\perp \cdot \underline{\kappa} = - \frac{1}{R_o} \left(\xi_r \cos \vartheta - \xi_\vartheta \sin \vartheta \right) \qquad (20)$$

yielding in the $v_{\|}$ integration in δW_h the contribution due to the resonances at

$$v_{\|} = \pm \frac{\ell}{2-\ell} v_A \text{ and } v_{\|} = \pm \frac{\ell}{2+\ell} v_A. \tag{21}$$

For the TAE with $\ell = 1$ the resonances occur at

$$v_{\|} = \pm v_A \tag{22a}$$

and

$$v_{\|} = \pm \tfrac{1}{3} v_A. \tag{22b}$$

The second resonance is not included in the work of Fu and Van Dam (1989). For the EAE with $\ell = 2$ the resonances occur at

$$v_{\|} = \pm \tfrac{1}{2} v_A \tag{23a}$$

$$v_{\|} = \pm \infty. \tag{23b}$$

By assuming a simple integrable equilibrium distribution for the core plasma in form of a Maxwellian distribution and for the α-particles in form of the usual slowing-down distribution eventually the result is obtained

$$\gamma / \omega_G = q_G^2 \left\{ \beta_\alpha \left(n q_G \delta_\alpha H_\alpha - G_\alpha \right) - 0.5 \, \beta_c \left(G_j + G_e \right) \right\}, \tag{24}$$

where the functions H_α, G_α (evaluated for a slowing down distribution for the a's) and G_i, G_e (evaluated for a Maxwellian for the core ions and electrons) occur together with the normalised α-pressure gradient length δ_α defined as the ratio of the poloidal Larmor radius and the α-pressure gradient length. The functions depend on $\lambda_\alpha = v_A / v_\alpha$ and $\lambda_j = v_A / v_{Tj}$ (for detail see Betti and Freidberg, 1992).

This result of Betti and Freidberg for the growth rate takes into account the α-particle drive and the background electron and ion Landau damping. Due to the $v_{\|} = \frac{1}{3} v_A$ resonance the ion Landau damping

$$G_i \propto e^{-\lambda_i^2/9} = e^{-1/9\beta i} \tag{25}$$

becomes dominant for large core beta. The numerical evaluation of Eq. (24) includes detailed JET profiles as obtained from TRANSP simulations together with the self-consistent fusion cross-section and slowing down of the α's.

The application for the JET preliminary tritium experiment takes into account the actual equilibrium and the profiles from discharge #26148. The gradient scale length $L_\alpha = (d\ell n\, P_\alpha/d_r)^{-1}$ has a minimum at $r_G/a \approx 0.47$.

Evidently, the alpha drive initially increases linearly with n up to an optimal number corresponding to the radial mode width becoming of the order of the radial alpha particle orbit width, $\Delta_b \sim q\rho_\alpha$. In JET, where $\Delta_b \sim$ 5-10cm the condition $\Delta_b \leq \Delta_n$ is satisfied typically for $n \leq 5$. Kinetic effects produce additional damping at high m. In particular, trapped electron collisional damping scales at high-m numbers as $\gamma_e / \omega_G \propto -m^2$ and provides thus a cut-off for high-mode number instabilities (Govelenkov and Sharapov, 1992 and Fu and Cheng, 1992). These conditions lead us to conclude that the Alfvén gap modes with toroidal mode numbers $n \geq 6$ are very hard to excite in foreseen JET DT experiments.

The gap structures and the continuum damping for perturbations with n = 1 to 5 have been investigated. An example of the gap structure for n = 3 is shown in Fig. 3 using the plasma parameters, in particular the density and q profiles, of the JET discharges #26148 (PTE1) and #26087 (JET best performance). The gap which is generated by the coupling of the m = 3 and 4 harmonics is located at the position of minimum L_α at $r_G/a = 0.47$. The corresponding q value is $q_G = 7/6$. It is evident that the radially nearest gaps at $q_G = 9/6$ (m = 4, 5) and at $q_G = 11/6$ (m = 5, 6) coincide in width and absolute value with the leading gap at $r_G/a = 0.47$, because the decrease in density compensates the increase in safety factor (i.e. $\rho^2 q \approx$ ct) for the actual discharge profiles. Therefore, the gaps thread through the plasma radially. From this study, the mode numbers have been selected which appear as most dangerous according to the following criteria: i) minimal or absent continuum damping; ii) "robust" gaps in the sense of surviving small changes (within estimated error bars) of the density and q profiles; iii) gaps located within 0.6 of the minor radius. In fact, the resonant α-particle contribution is most significant near the gap location and β_α drops to a negligible value for $r/a \geq 0.6$.

Marginal stability curves for the selected mode numbers have been obtained with a separate code based on the dispersion relation given in Eq. (24). This analysis

yields that the toroidicity - induced Alfvén gap eigenmode (TAE) with n = 3, and dominant poloidal harmonics m = 3, 4 is the most dangerous one for the parameters of these two discharges. In particular, for the PTE1 experiment, we have utilised the actual experimental values of deuterium, tritium and impurity densities. In the second case corresponding to the best performance in JET (#26087), we have simulated results assuming an equal concentration of deuterium and tritium. In both cases the alpha pressure profile has been evaluated by TRANSP which includes beam-beam and beam-plasma thermonuclear reactions, as well as thermal-thermal reactions (Balet et al., 1993).

The results of our analysis are summarised in Figs. 5 and 6 showing marginal stability curves in the $\beta_{\alpha G}$ - v_α/v_{AG} plane for the n = 3, m = 3, 4 TAE mode shown in Fig. 3b). Here v_{AG} and $\beta_{\alpha G}$ denote the Alfvén velocity and alpha particle beta at the gap location where $q_G = (m + \frac{1}{2})/n = \frac{7}{6}$, which is estimated to be at $r_G/a = 0.47 \pm 0.04$. The impurity mass density is included in the definition of v_A,

$$v_A = \frac{B_T}{\sqrt{\mu m_H \left(2n_D + 3n_T + 4n_\alpha + 10n_{imp} + 2n_{fastD} + 3n_{fastD}\right)}}, \qquad (26)$$

while $v_\alpha = (2E_\alpha/ma)^{1/2}$ with $E_\alpha = 3.5$MeV. Thus the abscissa is proportional to the square root of the electron density. The stability boundary results from the balance between the alpha particle drive and the Landau damping due to the electrons and bulk ions, while the continuum and collisional electron dampings are negligible small in this particular case. The boundary is obtained by varying the electron density while keeping all the other relevant parameters fixed at their experimental values at the time where the α-particle production reaches its maximum. The relevant parameters are the gap radius, the electron and ion temperatures at the gap, the α-particle pressure scale length and Z_{eff}. The hatched regions in Figs. 5 and 6 reflect the sensitivity of the marginal stability curves to uncertainties in these parameters. The experimental values of these parameters (with error bars) are indicated in the figure captions. The figures also show the values of $\beta_{\alpha G}$ and v_α/v_{AG} at the time corresponding to the maximum of $\beta_{\alpha G}$. Note that for both cases $\beta_\alpha(0)/\beta_\alpha(r_G) \sim 10$.

The gradient scale length L_α has a second minimum closer to the magnetic axis at $r_G/a \simeq 0.20$ where $L_\alpha/a \approx 0.25$. At this position the α-particle pressure, $\beta_{\alpha G}$, is larger. Almost the same destabilisation is obtained for the n = 3 EAE displayed in

Fig. 4a) and for the n = 5 TAE shown in Fig. 4b). It is evident that these eigenfunctions are considerably narrower than the TAE of Fig. 3b). Thus we conclude that this global TAE with dominant m = 3 and 4 harmonics is indeed the most dangerous one.

The conclusion from this analysis is that α-particle driven global Alfvén modes were stable in the PTE1. This result is confirmed by ion cyclotron emission measurements, ICE (Cottrel et al., 1993), where no evidence from saturation in the ICE signal caused by anomalous α-particle losses was obtained during the high performance phase. The second result is that the global Alfvén eigenmodes should also be stable in a future 50:50 deuterium-tritium mix experiment at JET provided the same ion density as in #26087 (which is higher than that in PTE1) is obtained. Concerning the PTE1 it is evident that the small α-particle pressure, $\beta_\alpha \lesssim 2 \times 10^{-4}$ is already sufficient to drive an instability. However, the Alfvén velocity is too small for a strong particle-Alfvén wave interaction. However, the proximity of the relevant parameters to their marginal stability values indicates that the excitation of Alfvén gap modes in future JET experiments is a realistic possibility. In particular, on the basis of Fig. 6, the unstable domain may be accessed in future D-T experiments by operating at lower plasma density and higher ion temperatures. In this fashion the ratio v_α/v_{AG} can be decreased to its optimal value for instability while maintaining a significant level of alpha particle production.

When this stability analysis is applied to a typical ITER configuration it is found that the unstable domain is missed because the Alfvén velocity of the plasma is too small. If high densities with $n_e \gtrsim 1.5 \times 10^{14} cm^{-3}$ can be achieved then stability for TAE is predicted, despite the high α-particle pressure, $\beta_\alpha \sim 10^{-2}$. This is evident from Fig. 7, where the stability boundaries for n = 3 and 5 are plotted in dependence of n_e and $T_e = T_i$.

4. CONCLUSION

A hybrid kinetic-MHD model is applied to the destabilisation of global Alfvén waves by α-particles in JET tritium discharges via inverse Landau damping. Our model allows incorporation of actual profiles of JET discharges and of planned future 50:50, D-T discharges based on best D-D discharges (#26087). Typically, the n = 3 and m = 3, 4 TAE of the corresponding gap in the Alfvén continuum at $r_G/a \approx 0.40$ is found to be the most likely candidate for destabilisation. The continuum

damping in this case is (almost) absent and core plasma Landau damping is small.

The conclusion from this stability analysis is that α-particle driven global Alfvén waves were stable in the PTE1 experiment and should also be stable in a future 50:50 D-T mix discharge aiming at break-even, $Q_{DT} \sim 1$. In this future experiment it is essential to maintain the same ion density as in discharge #26087. Since the α-pressure, $\beta_\alpha \sim (0.5 - 1) \times 10^{-3}$, is sufficiently large to drive instabilities the unstable domain is entered when $V_\alpha/V_A < 1.5$ as indicated in Fig. 6. In smaller tokamaks (DIII-D and TFTR) where the α's are barely confined significant α-particles losses are expected when global Alfvén waves become unstable. However, JET due to its small ripple and large volume, yields good α-particle confinement. Therefore, the plasma should evolve to parameters near marginal stability, the hatched region of Fig. 6, with the effect that the α-particle density is broadened (i.e. L_α enlarged) but the α's are not lost immediately. This conjecture is consistent with the surprisingly small losses of tritons during sawtooth crashes as observed in the neutron production rate (Marcus et al., 1993).

It is emphasised that the loss of energetic ions is difficult to assess theoretically. The predicted threshold in the amplitude of the perturbed magnetic field for enhanced turbulent α-losses varies from $\delta B_r/B_o \approx 10^{-5}$ to 10^{-4}, when different assumptions on the eigenfunction structure are made. Therefore it is essential to validate such models by experiments. By utilising the saddle coils global Alfvén waves can be excited at JET independent of the energetic particle drive. In conjunction with a controlled destabilisation by means of RF heating losses of MeV ions can be triggered. Finally, in the future JET D-T phase emphasis should not only be devoted to maximise the performance, i.e. Q_{DT}, but also to study the α-particle losses in steady state, i.e. at marginal stability with respect to alpha particle drive.

REFERENCES

B. Balet, P.M. Stubberfield, D. Borca, J.G. Cordey, N. Deliyanakis, C.M. Greenfield, T.T.C. Jones, R. König, F.B. Marcus, M.F.F. Nave, D. P. O'Brian, F. Porcelli, G.J. Sadler, K. Thomsen, M. von Hellerman. 'Particle and Energy Transport during the First Tritium Experiments on JET', to appear in Nucl. Fus.

R. Betti and J.P. Freidberg, Phys. Fluids **34**, 1465 (1992).

J. Blum, E. Lazzaro, J. O'Rourke, B. Keegan, Y. Stephan, Nucl. Fusion **30** (1990), 1475.

C.Z. Cheng and M.S. Chance Phys. Fluids **29,** 3695 (1988).

G.A. Cottrell, V.P. Bhatnagar, O da Costa et al., "Ion Cyclotron Emission Measurements During JET Deuterium-Tritium Experiments", to appear in Nuclear Fusion.

G. Fu and J.W. van Dam, Phys. Fluids **B1**, 1949 (1989).

G. Fu and C.Z. Cheng, Phys. Fluid B, **B4**, 3722 (1992).

N. Govelenkov and S. Sharapov, Phys. Scripts **45**, 163 (1992).

G.T.A. Huysmans, J. PGoedbloed and W. Kerner (1991) Europhysics 2nd Int. Conf. on Computational Physics, Amsterdam, 1990, CP90 (Edited by A. Tenner), p. 371. World Scientific, Singapore.

W. Kerner, S. Poedts, J.P. Goedbloed, G.T.A. Huysmans, B. Keegan and E. Schwarz (1991) Proc. of 18th European Conference on Controlled Fusion and Plasma Physics, Berlin. 3 - 7 June, IV.89-IV.92.

C.E. Kieras and J.A. Tataronis, J. Plasma Physics **28** 395 (1982).

F.B. Marcus (private communication).

S. Poedts and W. Kerner, Phys. Rev. Lett. **66** (22), 2871 (1991).

S. Poedts, W. Kerner, J.P. Goedbloed, B. Keegan, G.T.A. Huysmans and E. Schwarz in Plasma Phys. and Contr. Fusion **34**, 1397 (1992).

S. Poedts and E. Schwarz, Journ. Comput. Phys. **105** (1), 165 (1993).

F. Porcelli, R. Stankiewicz, W. Kerner and H. Berk, 'Solution of the Drift-Kinetic Equation for Global Plasma Modes and Finite Particle Orbit Width', JET-P(93)60, submitted to Phys. Fluids B.

The JET Team Nucl. Fusion **32** (2), 197 (1992).

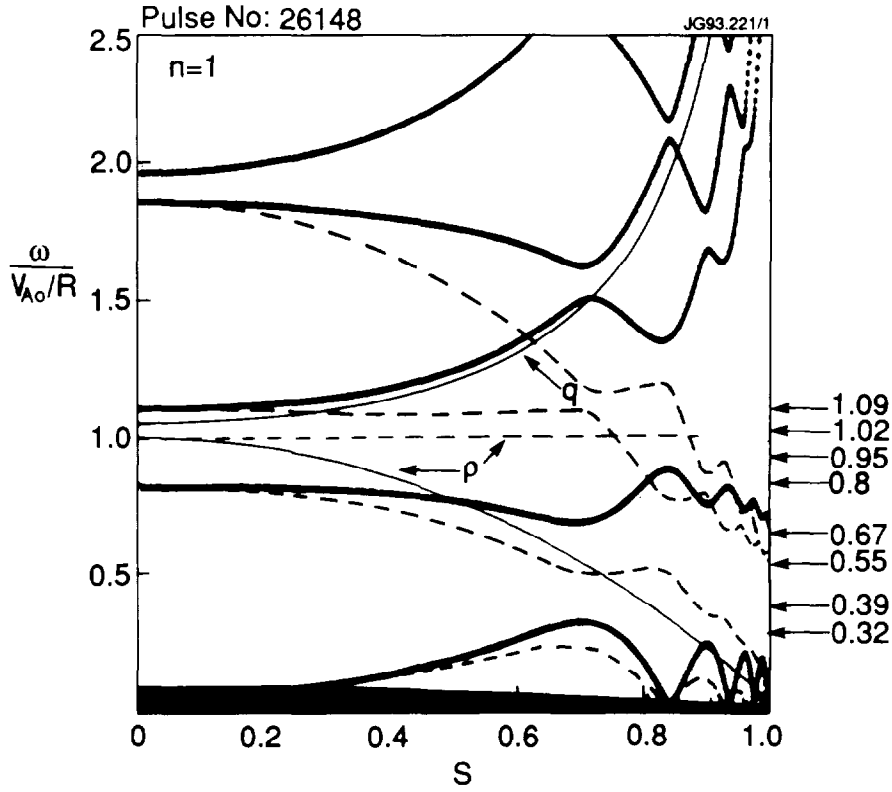

Fig.1. The radial dependence, $s = \sqrt{\psi / \psi_s}$, of the ideal MHD Alfvén continuous spectrum of a typical JET PTE1 discharge with n = 1, the global Alfvén eigenmodes are indicated by arrows.

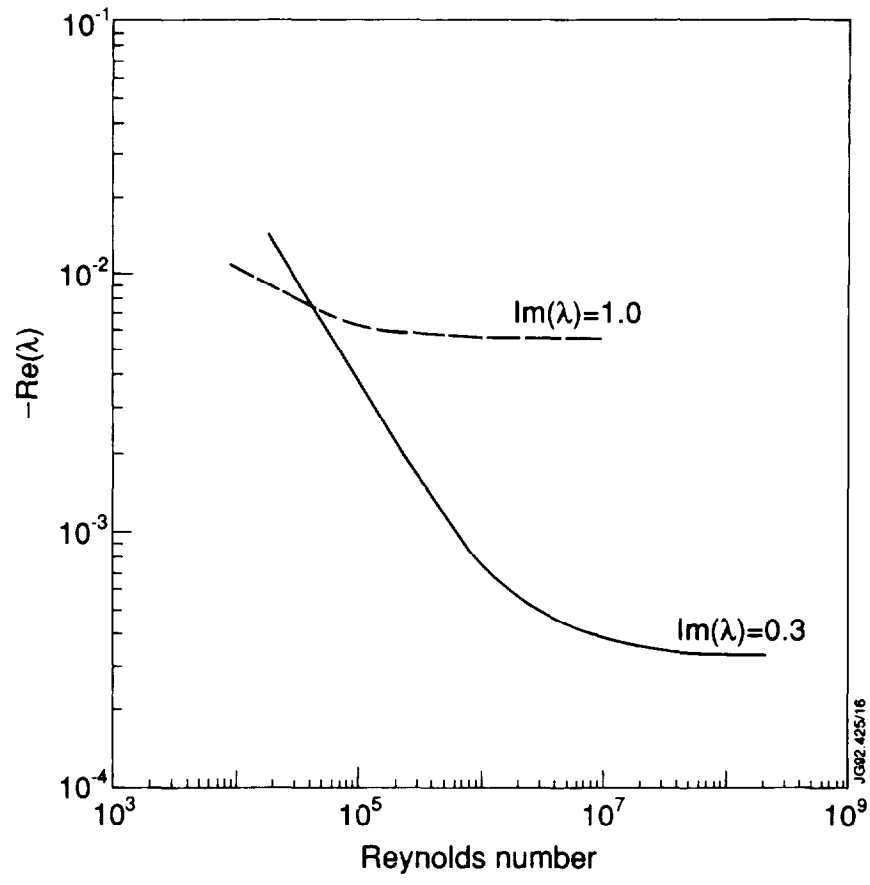

Fig. 2. Damping of two different Alfvén modes for constant density via interaction with continua in the limit of asymptotically small resistivity.

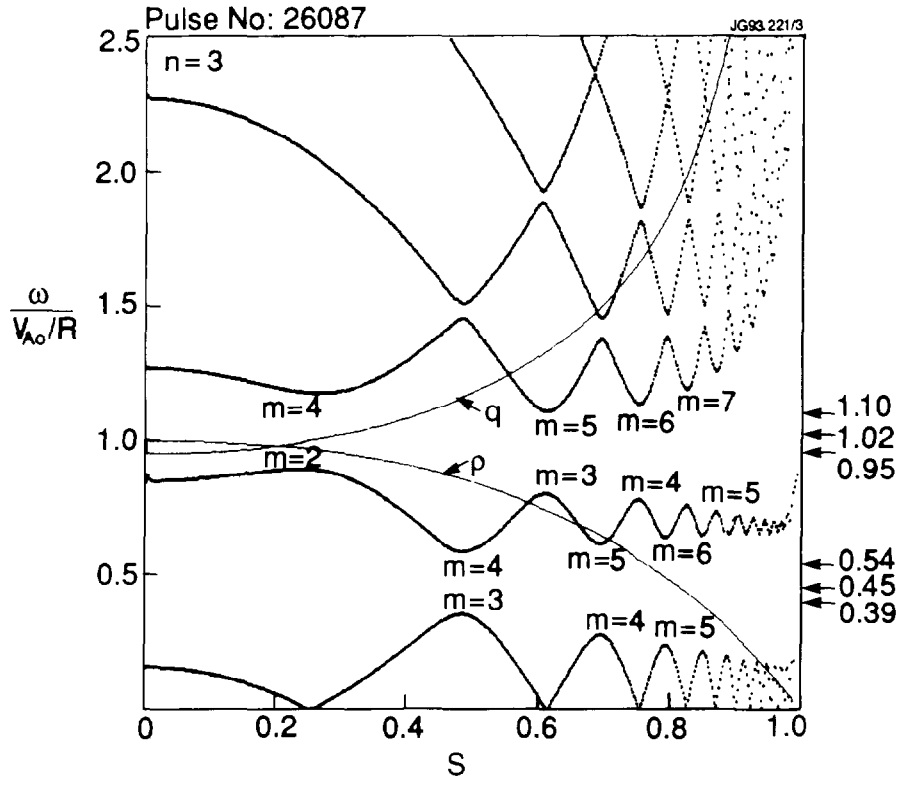

Fig.3. a) The radial dependence, $s = \sqrt{\psi / \psi_s}$, of the ideal MHD continuous spectrum of a typical JET PTE1 discharge with n = 3. The global Alfvén eigenmodes are indicated by arrows

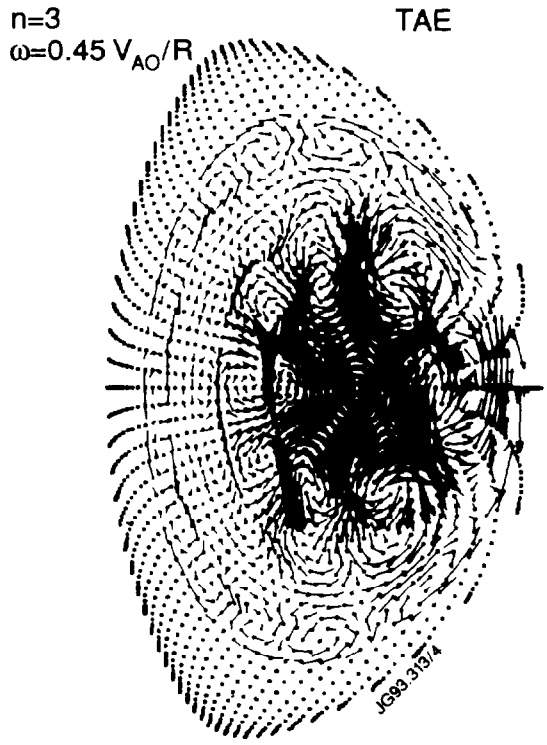

Fig.3. b) The eigenfunction for the TAE with $\omega = 0.45\ V_{AO}/R$.

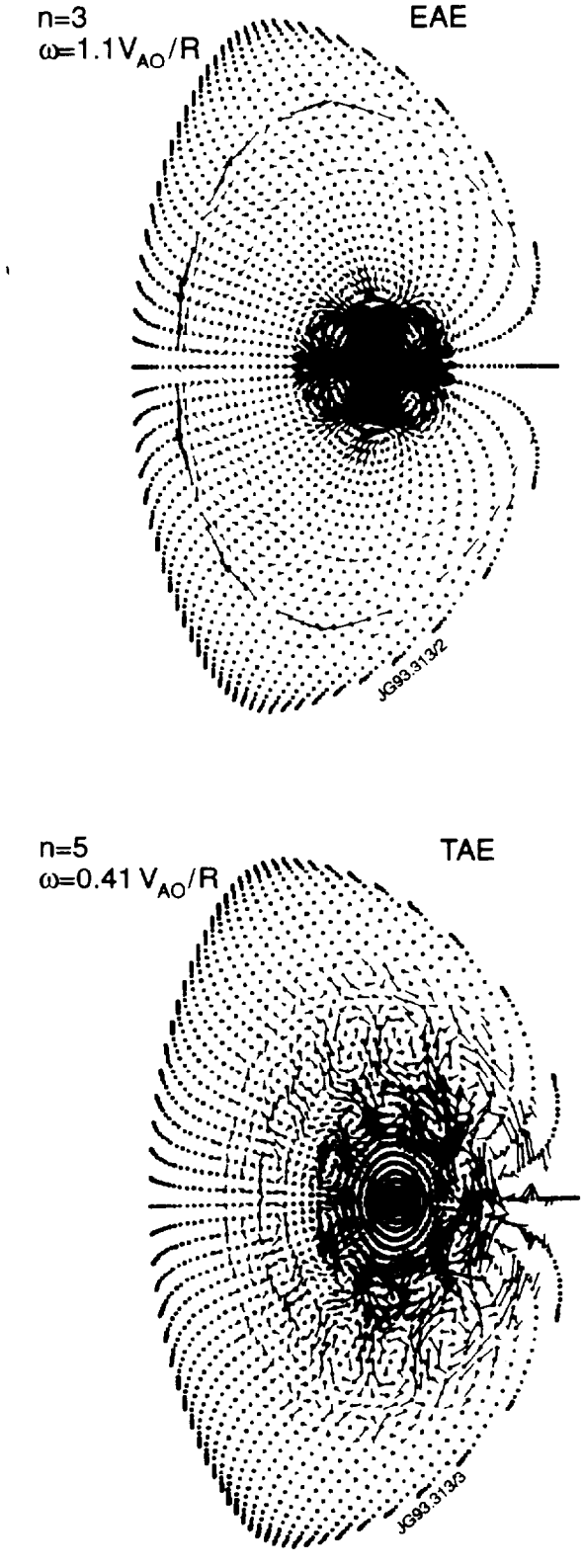

Fig.4. Global Alfvén eigenmodes for #26087 localised at s (≈r/a) = 0.20
a) EAE with n = 3 b) TAE with n = 5

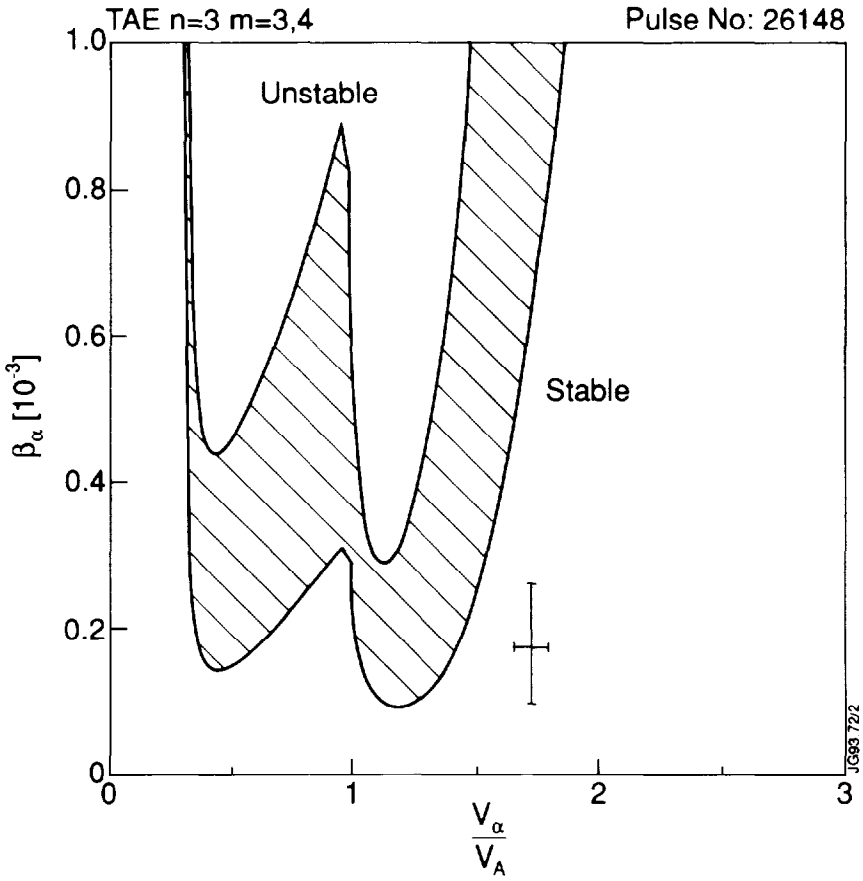

Fig.5. Stability boundary for discharge #26148 for the TAE mode with n = 3 and dominant m = 3 and 4 harmonics. Parameters at the q_G = 7/6 surface which is at $r_G/a = 0.47 \pm 0.04$ are as follows: (B_T = 2.8T):
#26148: $n_e = (3 \pm 0.3) \times 10^{19} m^{-3}$; $n_D = (1.84 \pm 0.2) \times 10^{19} m^{-3}$;
$n_T = (0.2 \pm 0.02)\ 10^{19} m^{-3}$; $T_i = (11 \pm 1)$ keV; T_e (7.5 ± 0.5) keV: $L_\alpha/a = 0.15 \pm 0.05$; $\beta_\alpha = (1.7 \pm 0.7) \times 10^{-4}$. The hatched region reflects the sensitivity of the marginal stability curve to variations of the relevant parameters within the corresponding error bars. The indicated values of $\beta_{\alpha G}$ and v_α/v_{AG} corresponds to the maximum value of β_α during the discharge evolution.

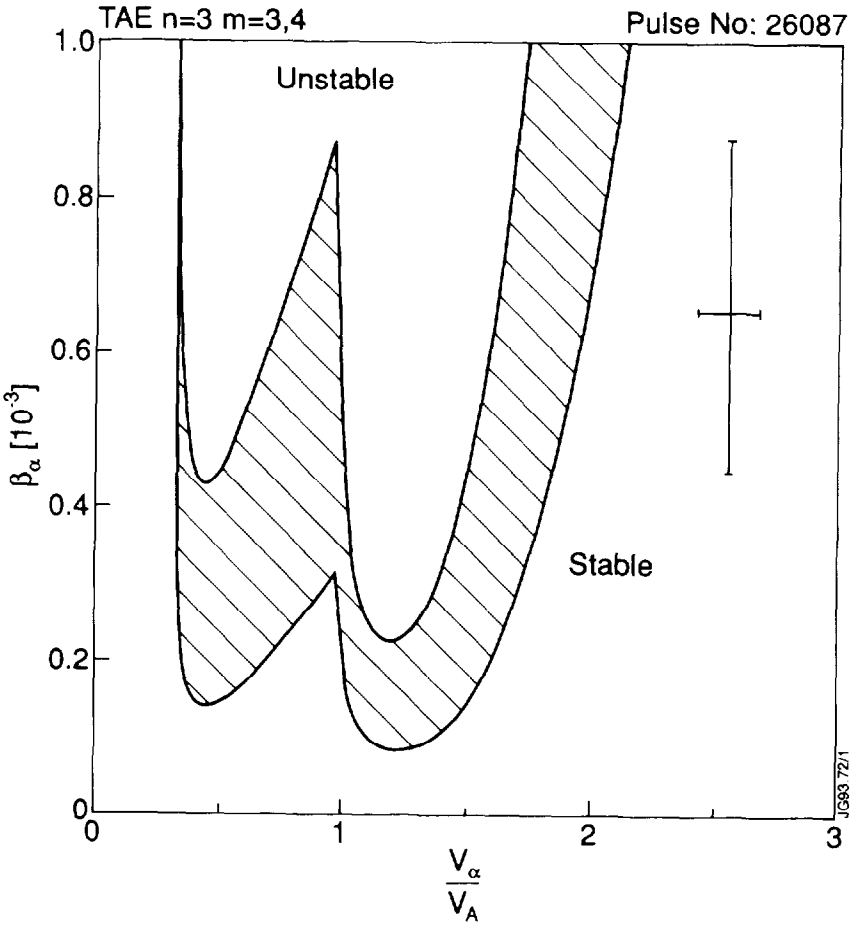

Fig.6. Stability boundary for discharge #26087 for the TAE mode with n = 3 and dominant m = 3 and 4 harmonics assuming $n_D \sim n_T$. #26087: $n_e = (4.8 \pm 0.4) \times 10^{19}m^{-3}$; $n_D = (1.8 \pm 0.2) \times 10^{19}m^{-3}$; $n_T = (1.9 \pm 0.2)10^{19}m^{-3}$; $n_i = (1.8 \pm 0.2) \times 10^{18}m^{-3}$, $T_i = (9.5 \pm 0.5)$ keV; $T_e = (8.2 \pm 0.5)$ keV; $L_\alpha/a = 0.15 \pm 0.05$; $\beta_\alpha = (6.5 \pm 2.5) \times 10^{-4}$. The hatched region reflects the sensitivity of the marginal stability curve to variations of the relevant parameters within the corresponding error bars. The indicated values of $\beta_{\alpha G}$ and v_α/v_{AG} corresponds to the maximum value of β_α during the discharge evolution.

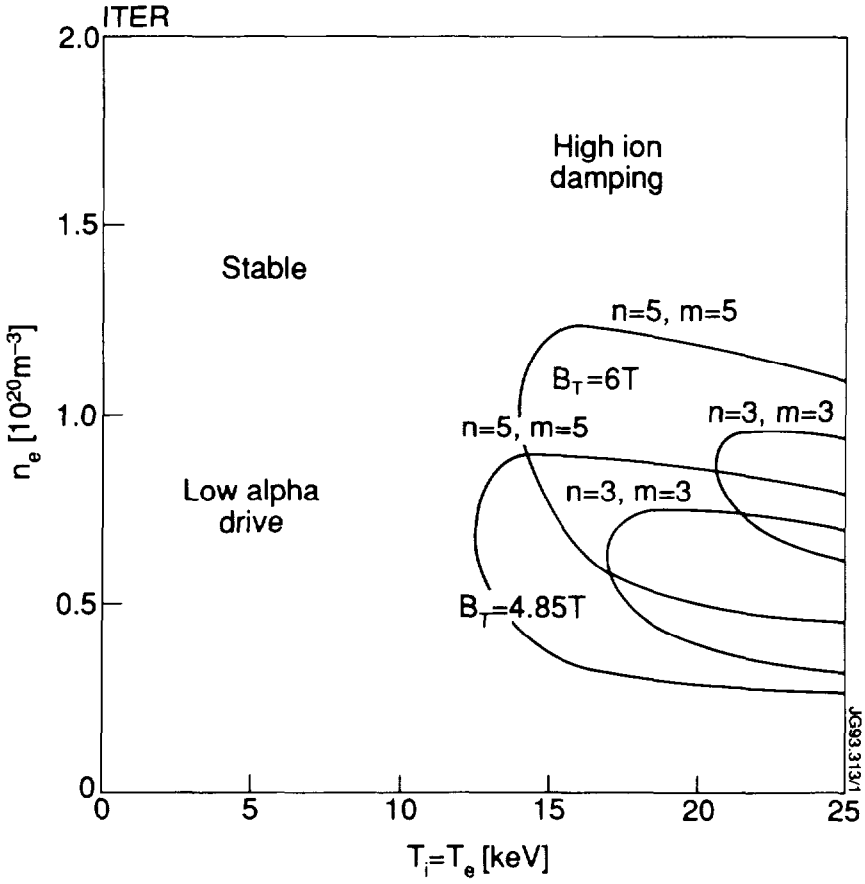

Fig.7. Stability boundary for ITER (r_o = 2.8m, R = 7.75m). If high density $n_e \geq 1.5 \times 10^{20}m^{-3}$ can be achieved then stability for TAE is predicted.